SPEED AND EFFICIENCY OF CHAOS DETECTION METHODS

Áron Süli
Department of Astronomy
Loránd Eötvös University
Pázmány Péter sétány 1/A
1117 Budapest, Hungary
a.suli@astro.elte.hu

Abstract In this article four chaos indicators were compared using the framework of the 2D standard map. These methods, namely the LCE, FLI, RLI and SALI may provide a global picture of the evolution of the mapping. Until now a detailed comparison of these methods have not been performed. This imperfection should be supersede. This is the aim of the paper.

Keywords: Chaos detection methods – Standard map

1. Introduction

The problem to separate ordered and chaotic motion in dynamical systems, especially in one with many degrees of freedom, is a fundamental task in several area of modern research. In order to determine the type of an initial condition in the phase space one needs fast and reliable tools. These tools are extremely useful in those cases when the inspected dynamical system has more than two degrees of freedom and therefore it's phase space can't be explored in a direct way or the classical method of Poincaré surface of sections can not be applied.

The mathematical foundation of the theory of Lyapunov characteristic exponents (hereafter LCE) arose progressively in the literature. The use of such exponents dates back to Lyapunov [9], but was firstly applied by [11] to characterize trajectories. In his paper Oseledec provides a general and simple way to compute not only the largest, but all the LCEs. The first numerical characterization of stochasticity of a phase space trajectory in terms of divergence of nearby trajectories was introduced by the classical paper of [6]. They found that two orbits initially close diverge either linearly or exponentially depending

Table 1. Enumeration and classification of the methods.

analysis of the orbits	**analysis of the tangent vector**
1. Poincaré surface of section	1. Lyapunov characteristic exponents (LCE) [9]
2. Frequency analysis method (MFT) [8]	2. Generalized Lyapunov indicators (GLI) [3]
3. Low frequency power spectra [16]	3. Spectra of stretching numbers [14]
4. Sup-map method [8]	4. Spectra of helicity and twist angles [2]
5. Spectral analysis method (SAM) [10]	5. Fast Lyapunov indicators (FLI) [4]
	6. Spectral distance [15]
	7. Mean exponential growth of nearby orbits (MEGNO) [1]
	8. Relative Lyapunov indicator (RLI) [12]
	9. Smaller alignment index (SALI) [13]

on whether the initial points lie in an integrable or in a stochastic region of the phase space.

In the last three decades much work, both analytical and numerical have been performed to investigate the chaotic properties of classical dynamical systems. In addition to the elaborated theory of LCE several new methods have been developed in order to establish the true nature of an orbit in the shortest possible timespan. These methods are based on the analysis of the orbits, or on the time evolution of the tangent vector i.e. the solution of the linearized equations of motion. Accordingly the methods can be classified in two groups (see Table 1).

In this paper the LCE, the FLI, the RLI and the SALI methods will be investigated and compared in the framework of the 2D standard map, defined by the

$$\begin{aligned} x_{i+1} &= x_i + y_i, \\ y_{i+1} &= y_i - K\sin(x_i + y_i), \end{aligned} \qquad \texttt{mod } 2\pi \tag{1}$$

equations, where $K \geq 0$ is the non-linearity parameter. Throughout the paper the $K = 0.3$ case is considered. For this value of the non-linearity parameter the complete phase space of the system and the vicinity of the hyperbolic point (π,0) is depicted in Fig. 1.

In Section 2 the methods are shortly described. In Section 3 the speed of the methods are presented and compared, and also their dependence on the initial tangent vector ξ is discussed. In Section 4 the results are summarized.

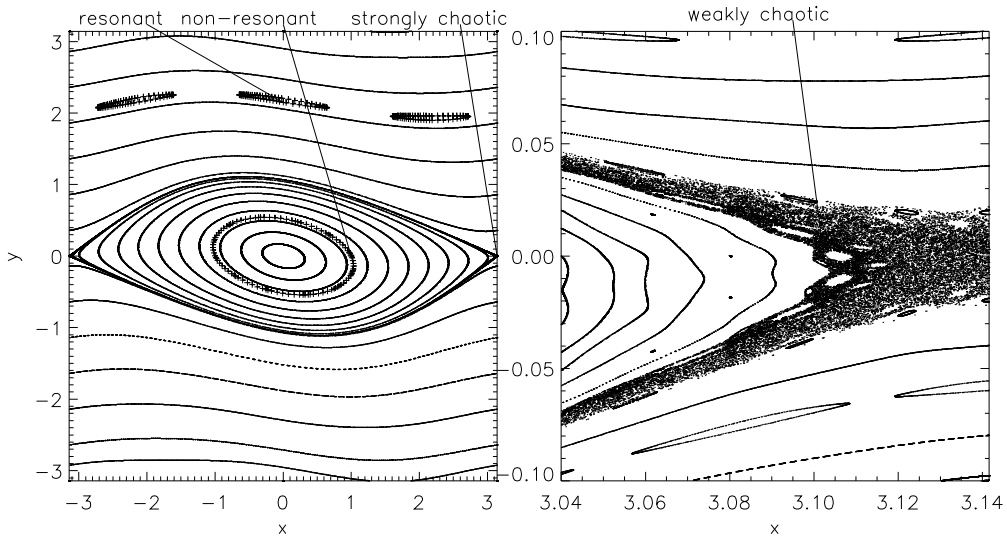

Figure 1. The phase space of the standard map for $K = 0.3$. The vicinity of the hyperbolic point is enlarged to visualize the initial condition of the weakly chaotic orbit.

2. Methods: LCE, FLI, RLI and SALI

Let us briefly review the definition of the different methods! The definition of the largest LCE for an initial value problem or mapping

$$\frac{\mathrm{d}\mathbf{y}(t)}{\mathrm{d}t} = \mathbf{f}(t,\mathbf{y}), \quad \mathbf{y}(0) = \mathbf{y}_0, \tag{2}$$

$$\mathbf{y}_{i+1} = \mathbf{M}(\mathbf{y_i}), \quad \mathbf{y}_{i=0} = \mathbf{y}_0, \tag{3}$$

is given by

$$\mathtt{LCE} = \lim_{t\to\infty} \frac{1}{t-t_0} \log \frac{||\xi(t)||}{||\xi(0)||} = \lim_{t\to\infty} \gamma(t,\mathbf{y}_0,\xi_0), \tag{4}$$

where $\xi(t)$ is the solution of the first order variational (i.e. linearized) equations and the function $\gamma(t,\mathbf{y}_0,\xi_0)$ measures the mean rate of divergence of the orbits. The linearized equations are:

$$\frac{\mathrm{d}\xi(t)}{\mathrm{d}t} = \frac{\partial \mathbf{f}(t,\mathbf{y})}{\partial \mathbf{y}}\xi, \quad \xi(0) = \xi_0, \tag{5}$$

$$\xi_{i+1} = \frac{\partial \mathbf{M}(\mathbf{y_i})}{\partial \mathbf{y}}\xi_\mathbf{i}, \quad \xi_{i=0} = \xi_0. \tag{6}$$

The value of LCE reveals the sensitivity of the given trajectory to the initial conditions. The problem of the LCE is that it is defined as a limit. Though the largest LCE can be calculated up to a (very) large time T but the limes as t tends to infinity cannot be evaluated numerically. Therefore the function $\gamma(t,\mathbf{y}_0,\xi_0)$ is called the Lyapunov characteristic indicator (hereafter LCI),

which is a finite estimate of the LCE. Thus the evolution of LCI(t, x_0, ξ) is followed up and we plot logLCI versus $\log t$. If the curve has a negative constant slope, the trajectory is ordered; if it exhibits an inflection of the slope, which comes close to 0 and the function converges to a certain value, the orbit is chaotic.

The FLI was introduced as the initial part (up to a stopping time t_s) of the LCE's computation:

$$\texttt{FLI}\left(\xi(0), \mathbf{y}_0, t_s\right) = \sup_{j=1,\ldots,n} ||\xi_j(t)||, \tag{7}$$

where n is the dimension of the phase space. To determine the FLI of a given orbit one has to follow the evolution of n tangent vectors, which initially span an orthogonal basis of the tangent space. The FLI tends to zero in both ordered and chaotic regions as the number of iterations (in the case of maps) or the time (in Hamiltonian systems) increases, but on completely different time scales which makes it possible to separate the phase space.

The RLI was introduced as the difference between the LCIs of two initially nearby orbits:

$$\texttt{RLI}(\xi(0), \mathbf{y}_0, t_s) = \frac{1}{t}|\mathrm{LCI}(\xi(0), \mathbf{y}_0, \mathrm{t_s}) - \mathrm{LCI}(\xi(0), \mathbf{y}_0 + \Delta \mathrm{y}, \mathrm{t_s})|, \tag{8}$$

where Δx is the distance in phase space between the two orbits.

The basic idea behind the SALI method is the intoduction of a simple quantity that indicates if a tangent vector is aligned with the direction of the eigenvector corresponding to the maximal LCE.

In order to check the directions of the vectors, the evolution of two tangent vectors are followed. The parallel and the antiparallel alignment indices are respectively defined as

$$d_- = ||\xi_1(t) - \xi_2(t)||, \quad d_+ = ||\xi_1(t) + \xi_2(t)||.$$

The SALI is defined as the minimum of the indices:

$$\mathrm{SALI}(t) = \min\left(d_+, d_-\right). \tag{9}$$

SALI tends to zero when to orbit is chaotic, and to a non-zero positive value when to orbit is regular. In the special case of 2D maps, SALI tends to zero for every initial conditions but follows completely different time rates for ordered and chaotic orbits.

3. Efficiency and dependence

Both the efficiency and the dependence was study in the case of four different kinds of orbits. The initial conditions are given in Table 2, the corresponding orbits are plotted on Fig. 1.

Table 2. Classification of the orbits and initial conditions.

Orbit			
Ordered		Chaotic	
non-resonant	resonant	strongly	weakly
(1;0)	(0;2.15)	(3.14;0)	(3.1024048;0)

First the number of iterations needed to establish with certainty the nature of an orbit was determined. An orbit can be classified as ordered (regular) or chaotic. An ordered orbit can be divided into two subclasses: non-resonant and resonant. An orbit is non-resonant, when there does not exist such linear combination of the frequencies of the motion which vanishes, otherwise the orbit is resonant. The chaotic orbits may be further classified, accordingly to the rate of divergence of nearby orbits. In this context, one can speak about strongly and weakly chaotic orbits. If two initially nearby trajectories diverge fast, the orbit is strongly chaotic, if the divergence is slow (comparing to the previous case), we speak about weakly chaotic or sticky orbit. The above classification is presented in Table 2, where also the initial conditions of the different orbits for the standard map are listed.

In Fig. 2 the time evolution of the four indicators are plotted for the above mentioned different kinds of orbits. The stopping time was set to 10^9 iterations. In the case of FLI, RLI and SALI an additional stopping criteria was used: whenever the FLI, RLI or SALI reached 10^{20}, 10^{-20} or 10^{-16}, respectively the computation was stopped.

Between 1 and some times 10 iterations none of the methods is capable to establish the type of the orbit: all four curves are overlapping each other inhibiting the classification. At the earliest at 100 iterations the strongly chaotic orbit can be separated from the ordered one, but with certainty the classification can be done at 1000 iterations.

In the case of LCI, FLI and SALI the indicator corresponding to the weakly chaotic orbit (dotted line) follows exactly the curve belonging to the strongly chaotic orbit (solid line) for the first 10 iterations. Afterwards the weakly chaotic curve essentially follows the curves corresponding to the ordered orbits for approximately 10^6 iterations. In the case of LCI the classification is only possible after approximately 10^6 iterations, when the curve has a turning point, and its slope becomes zero. It is worth noting, that after some 10^8 iterations the LCI suddenly jumps form 1.21×10^{-5} to 6.03×10^{-3}, than it climbs to 2.55×10^{-2} which is very close to the value belonging to the strongly chaotic orbit (3.45×10^{-2}). This is a numerical evidence, that both orbits originate in the chaotic domain. In the case of the FLI approximately 2×10^6, whereas in the case of the SALI about 9×10^5 iterations are needed for the assignment.

In the case of the RLI, the weakly chaotic curve does not follow any other, but it wildly oscillates around 10^{-12}. Between 100 and 1000 iterations it overlaps with the ordered curves, beyond 10^6 it goes close to the strongly chaotic curve. The classification is possible after 10^4 iterations.

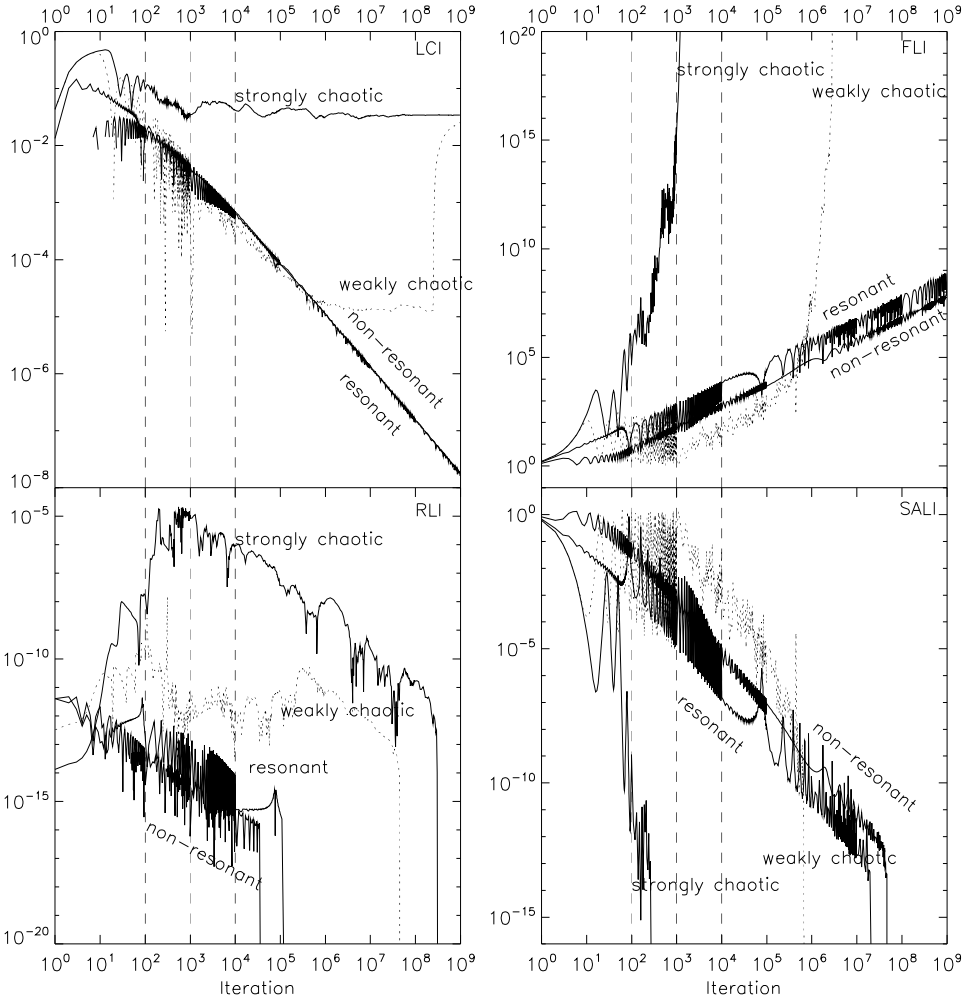

Figure 2. Variation of the CIs with the number of iterations for four kinds of orbits of the standard map. The dotted curves correspond to the weakly chaotic orbit.

A careful examination of the curves in Fig. 2 allows one to distinguish also between resonant and non-resonant motion. Although the curves corresponding to a non-resonant and a resonant motion are separated in the case of FLI, RLI and SALI, the oscillations prevent definite distinction between the two cases. Therefore, following the idea of [5], the definitions are replaced by their running average

$$\widehat{\mathrm{CI}}(t) = \frac{1}{2N} \sum_{k=i-N}^{i+N} \mathrm{CI}_k, \tag{10}$$

where CI denotes one of the methods and N is the width of the running window. In the following $N = 50$ was used.

In Fig. 3 the running average of the indicators are shown. In the case of LCI and SALI the two curves can not be distinguished from each other, whilst the FLI and RLI curves are well separated after 100 iterations. It appears clearly that using $\widehat{\mathrm{FLI}}(t)$ and $\widehat{\mathrm{RLI}}(t)$ resonant and non-resonant motion are clearly separated. We note that the corresponding lines appear to be parallel. This averaging technique does not influence the behaviour of the indicators in the case of chaos.

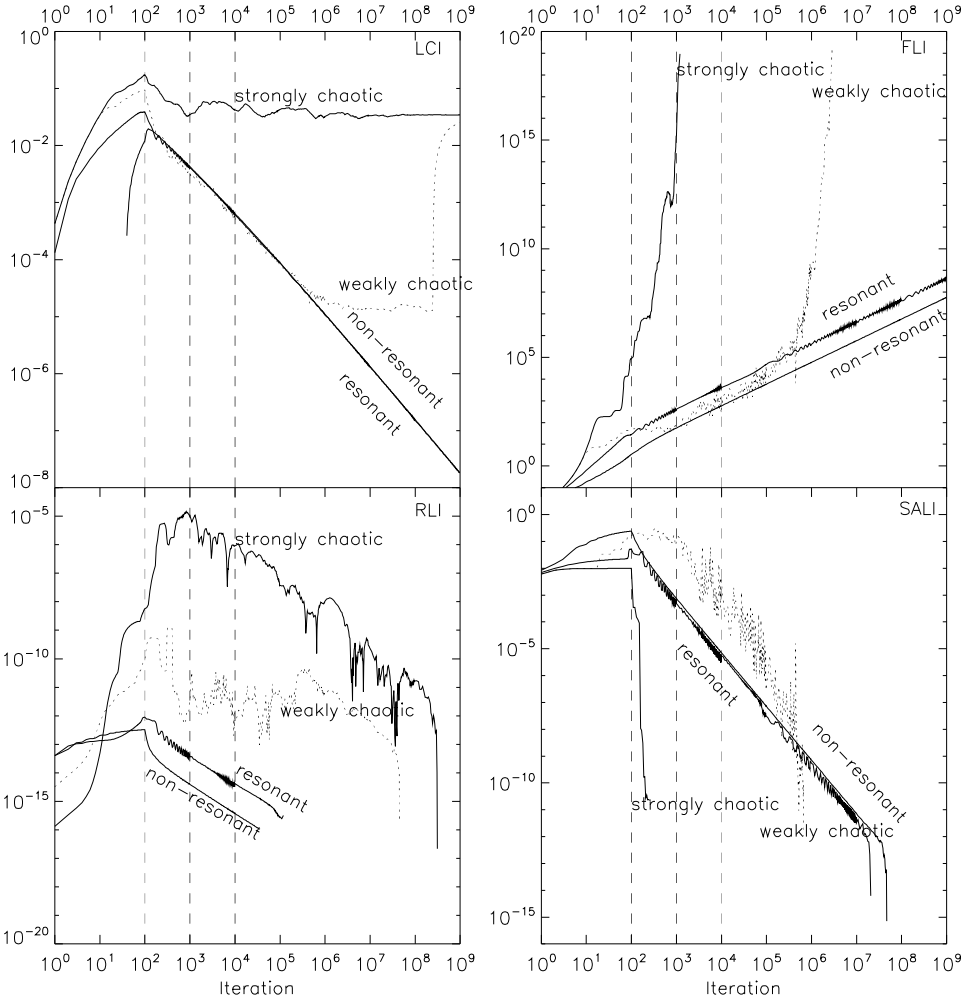

Figure 3. Variation of the $\widehat{\mathrm{CI}}(t)$s with the number of iterations for four kinds of orbit of the standard map.

It is obvious, that the methods are sensitive to the initial direction of the tangent vector $\xi(0)$. To quantify therefore the methods' dependence on the direction of $\xi(0)$, the tangent vector is rotated, and the indicator is calculated up to several stopping times. This dependence is confirmed in Fig. 4 in which the values of the CIs are plotted against the angle ϕ, for the resonant, non-

resonant and chaotic orbits for 1000 iterations. The ϕ is the angle between $\xi(0)$ and the (1,0) vector (x-axis). From Fig. 4 it is obvious that these values are far from being constant when varying the angle ϕ. In order to plot all four curves together, a normalization was performed, i.e. the CI values were divided by their maximum value (see Table 3).

The normalized curves have extremum at the same ϕ, which is a natural consequence of that, that all four methods are based on the evolution of the tangent vector. The LCI and RLI are periodic with π, since these methods are based on one $\xi(0)$, while the FLI and SALI are periodic with $\pi/2$, because they are based on two tangent vectors which are initially perpendicular to each other.

Table 3. Dependence and relative variation for the resonant orbit.

	LCI	**FLI**	**RLI**	**SALI**
max	0.00653987	692.198	5.77967e-15	0.00307465
min	-0.00075530	489.790	2.97609e-15	4.17417e-06
Δ_{CI}	1.937	1.15	1.288	3.867
ϕ_{max}	81°.5 (261°.5)	81°.5 (171°.5)	171°.5 (351°.5)	81°.5 (171°.5)
ϕ_{min}	171°.5 (351°.5)	36°.5 (126°.5)	171°.0 (351°.0)	36°.5 (126°.5)
$\Delta\phi$	180°	90°	180°	90°

In Table 3 the maximum and minimum values for the resonant orbit are listed. Introducing the quantity

$$\Delta_{\mathrm{CI}} = 1 - \log_{10}\left(\frac{\min(CI)}{\max(CI)}\right), \tag{11}$$

also the measure of dependence was determinded. According to the third line of Table 3, we see that the SALI has the largest, and the FLI has the smallest value which could already be observed in Fig. 4.

4. Summary

In this article a possible classification of the chaos detection techniques was given, and four methods, namely the LCI, the FLI, the RLI and the SALI were briefly described in Section 2. These methods were compared using the 2D standard map. The efficiency of these techniques was tested via applying them to four different types of orbits. It was shown that all the four methods are capable to distinguish between strongly chaotic and ordered motion after approximately 100 iterations. To reveal the true nature of a weakly chaotic orbit, it turned out that the new methods are not superior to the classical method of LCI: in short time interval they failed to properly classify the orbit. This is because the weakly chaotic orbit pretends regular behaviour for a priori un-

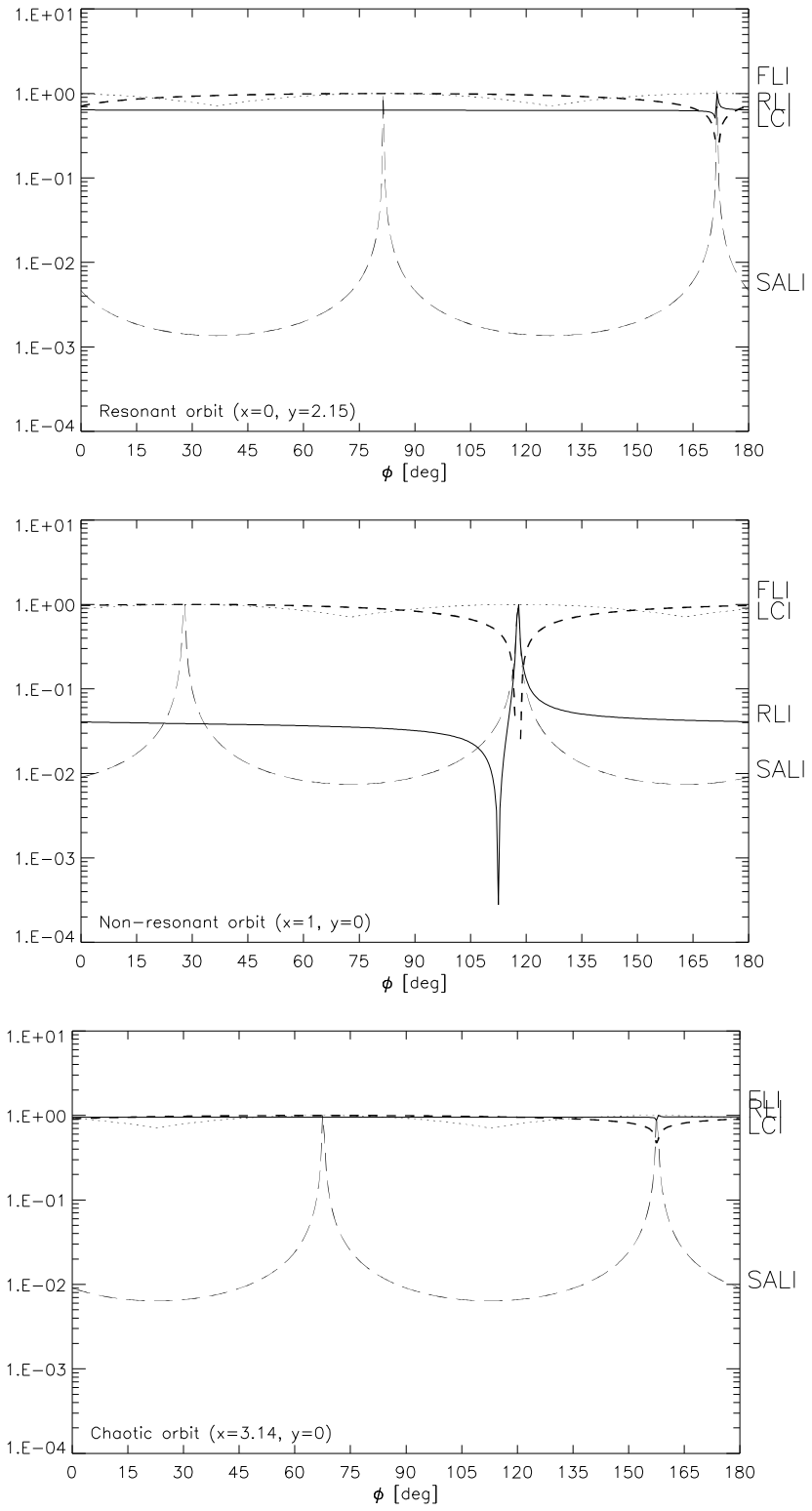

Figure 4. Variation of the CIs as a function of the initial direction of the tangent vector(s) for the resonant (top), non-resonant (middle) and chaotic (bottom) orbit.

known time interval. The length of this time interval may be considered as the measure of chaos: the longer the interval the weaker the chaos is.

Introducing the running average technique, the $\widehat{\mathrm{FLI}}$ and the $\widehat{\mathrm{RLI}}$ can separate between resonant and non-resonant orbits. This technique does not improve the capabilities of LCI and SALI.

The sensitivity of the methods to the initial direction of the tangent vector $\xi(0)$ was demonstrated and compared. It was shown for three types of orbits that the CIs have extremum at the same ϕ, which is the angle between $\xi(0)$ and the x-axis. The LCI and RLI are periodic with π, while the FLI and SALI are periodic with $\pi/2$. With the definition of Δ_{CI} the dependence of the methods were quantitatively described. The least sensitive is the FLI, the most one is the SALI.

In the future it is necessary to calculate these methods on a large portion of the phase space, and also to extend these calculations for Hamiltonian dynamical systems.

Acknowledgments

The support of the Austrian-Hungarian Scientific and Technology Cooperation, grant number A-12/04 is acknowledged.

References

[1] Cincotta, P.M. and Simo C.: 2000 "Simple tools to study global dynamics in non-axisymmetric galactic potentials - I", *Astron. Astrophys. Suppl. Ser.* **147**, 205.

[2] Contopoulos, G., Voglis, N.: 1996 "Spectra of Stretching Numbers and Helicity Angles in Dynamical Systems" *Celest. Mech. & Dyn. Astron.* **64**, 1.

[3] Froeschlé, C., Froeschlé, Ch., Lohinger, E.: 1993, "Generalized Lyapunov characteristic indicators and corresponding Kolmogorov like entrophy of the standard mapping", *Celest. Mech. & Dyn. Astron.* **56**, 307.

[4] Froeschlé, C., Lega, E., Gonczi, R.: 1997 "Fast Lyapunov Indicators. Application to Asteroidal Motion" *Celest. Mech. & Dyn. Astron.* **67**, 41.

[5] Froeschlé, Claude; Lega, Elena: On the Structure of Symplectic Mappings. The Fast Lyapunov Indicator: a Very Sensitive Tool Celestial Mechanics and Dynamical Astronomy, v. 78, Issue 1/4, p. 167-195 (2000)

[6] Henon, M., Heiles, C.: The applicability of the third integral of motion: Some numerical experiments Astronomical Journal, Vol. 69, p. 73, 1964

[8] Laskar, J.: 1990, "The chaotic motion of the Solar System: A numerical estimate of the size of the chaotic zones", *Icarus* **88**, 266-291.

[8] Laskar, J.: 1994, "Large-scale chaos in the solar system", *Astr. Astrophys.* **287**, L9-L12.

[9] Lyapunov A. M.: (1907) Ann. Math. Studies 17, Princeton, 1947

[10] Michtchenko, T. A., Ferraz-Mello, S.: 1995 "Comparative study of the asteroidal motion in the 3:2 and 2:1 resonances with Jupiter. I. Planar model", *Astronomy and Astrophysics*, **303**, 945.

[11] Oseledec V. I.: Trans. Moscow Math. Soc. 19, 197, 1968

[12] Sándor, Zs., Érdi, B., Efthymiopoulos, C.: 2000 "The Phase Space Structure Around L4 in the Restricted Three-Body Problem", *Cel. Mech. & Dyn. Astron* **78**, 113.

[13] Skokos, Ch.: 2001 "Alignment indices: a new, simple method for determining the ordered or chaotic nature of orbits" *Journal of Physics A*, **34**, 10029.

[14] Voglis, N., Contopoulos, G. J.: 1994 "Invariant spectra of orbits in dynamical systems" *Journal of Physics A* **27**, 4899.

[15] Voglis, N., Contopoulos, G., Efthymiopoulos, C.: 1999 "Detection of Ordered and Chaotic Motion Using the Dynamical Spectra", *Cel. Mech. & Dyn. Astron* **73**, 211.

[16] Voyatzis G. and Ichtiaroglou S.: 1992 "On the spectral analysis of trajectories in near-integrable Hamiltonian systems", *J. Phys. A* **25**, 5931